Correlation of Microstructures and Process Variables in FSW HSLA-65 Steel

Of the FSW process heat indexes investigated, heat input provided the best correlation with post-friction stir weld microstructures

BY L. Y. WEI AND T. W. NELSON

ABSTRACT

The present study focuses on developing a relationship between process variables and postweld microstructure in friction stir welded HSLA-65 steel. Fully consolidated welds were produced in HSLA-65 steel using a PCBN convex-scrolled-shoulder-step-spiral (CS4) tool over a wide range of parameters. Microstructures in the nugget center (NC) are governed by lath bainite and with some polygonal/allotriomorphic grain boundary ferrite, which are highly dependent on heat input. Friction stir welded dependent variables are related with FSW independent variables by nonlinear relationship. Heat input is identified as the best parameter index. With increasing heat input, the volume of bainite decreases and the ferrite grain and lath sizes increase. A linear relationship was established between heat input and semiquantitative postweld microstructures.

Introduction

Friction stir welding (FSW) is a solid-state technology that has attracted considerable interest since it was invented at TWI in 1991. Friction stir welding utilizes a nonconsumable tool that is inserted into the abutting edges of the base metal. The rotating tool generates heat by friction and plastic deformation between itself and the base plate complete the joining process (Ref. 1).

Friction stir welding has shown distinct advantages over traditional arc welding. Because there is no melting, FSW produces less distortion and defects associated with cooling from liquid phase, such as liquidation-related cracking and porosity (Ref. 2). Additionally, FSW is a "green" technology in that it produces no arc radiation, no fumes, and no hazardous waste.

The FSW process can be used to join high-strength aluminum alloys that are difficult to weld with conventional arc welding. The intense plastic deformation at elevated temperature produces a fine equiaxed microstructure due to dynamic recrystallization (Refs. 3–5). As-welded 7075Al-T651 shows a reduction in yield and ultimate strengths in the weld nugget, which is associated with the coarsening of the very fine hardening precipitates (Refs. 3, 4). Rapid implementation of FS welded aluminum alloys into industry applications has motivated its application to other nonferrous materials, such as Mg (Ref. 6), Ti (Refs. 7, 8), and Cu (Refs. 9, 10).

Although most FSW research has focused on aluminum alloys, there is considerable interest in the application of this technology to steels. Several studies have reported on FSW of carbon and stainless steels. Friction stir welded carbon and ultrafine-grained plain low-carbon steels have shown increased strength in the stir zone due to refined microstructures and the formation of martensite and bainite (Refs. 11–13). Similarly, FS welded 304L stainless steel exhibits higher tensile properties than base metal (Ref. 14). It has also been reported that FSW significantly refines the grains in the stir zone of 2507 superduplex stainless steel while maintaining the 50/50 austenite/ferrite ratio in the weld (Ref. 15).

In recent years, there has been much interest in FSW of high-strength low-alloy (HSLA) type steel. High-strength low-alloy type steels are relatively new structural steels for use in applications requiring high strength, ductility, and good weldability, such as shipbuilding, oil and gas line pipe. High-strength low-alloy steels are manufactured by thermo-mechanical controlled processing (TMCP), which produces uniform refined microstructures providing superior combination of high-strength and excellent toughness (Ref. 16). In conventional arc welding of HSLA steel, the heat-affected zone (HAZ) is susceptible to hydrogen-assisted cracking (HAC). Moreover, significant loss of strength and toughness in the HAZ can seriously compromise the mechanical properties of the weld (Ref. 16).

Friction stir welding has offered distinct advantages relative to the arc welding of HSLA-type steels. Previous research demonstrated the feasibility of FSW HSLA 65 (Ref. 17), and X80 and L80 steels (Ref. 18), all of which exhibited satisfactory mechanical properties. Softening of the HAZ in HSLA 65 (Ref. 21) and X80 (Ref. 18) weldments were reported. Post-FSW microstructural analyses of HSLA 65 (Refs. 19–21), X80, and L80 (Ref. 18) were limited. In addition, the effect of FSW parameters on postweld microstructure and properties in HSLA steels has not been thoroughly investigated.

The influence of FSW parameters on the microstructure and mechanical properties has been studied by a number of investigators in Al and Mg alloys. Querin (Ref. 22) and Rodrigues (Ref. 23) found higher rotation speed resulted in finer microstructures in FSW AA2219-T87 and AA6016-T4. Afrin (Ref. 24) and Cao (Ref. 25) reported larger grain size and decreasing tensile properties at lower welding speed in FSW AZ31B magnesium alloy. Cui (Ref. 26) concluded the welding speed strongly affected the total size of the stir zone of A356 cast alloy. Pilchak (Ref. 27) showed the welding speed had an insignificant effect on grain size of FSW Ti-6Al-4V alloy.

Most research to date has tried to establish correlations between FSW independent variables (travel speed, rotation speed) with postweld properties. Research is limited on the investigation of the correlations between FSW dependent variables, e.g., power and heat input, and postweld characteristics. In traditional arc welding, it is common practice to correlate welding process parameters and mi-

KEYWORDS

Friction Stir Welding
HSLA-65 Steel
Nugget Center
Heat Indexes
Ferrite Grain Size
Bainite Lath Size

L. Y. WEI (lingyun.wei@ssab.com) *is with R & D, SSAB Americas, Mascatine, Iowa, and T. W. NELSON is with Mechanical Engineering Dept., Brigham Young University, Provo, Utah.*

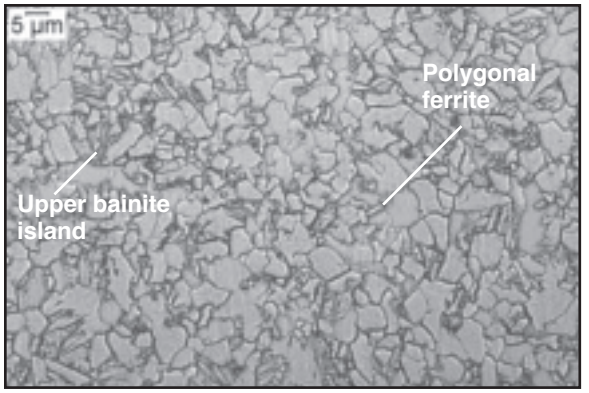

Fig. 1 — Grain structures of the base metal.

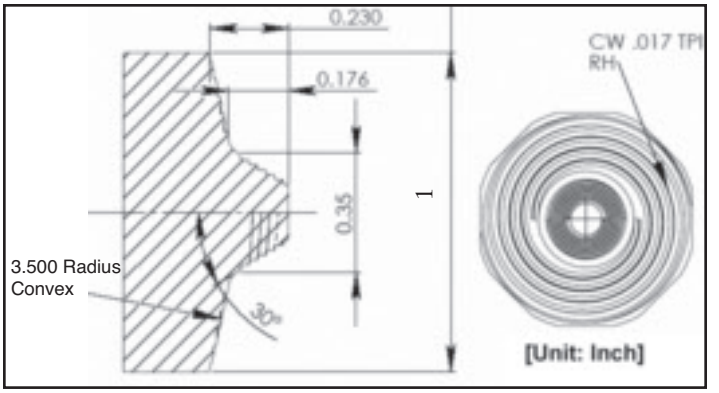

Fig. 2 — Geometry of CS4 tool used in the welding.

crostructures with weld heat input. Correlations between HAZ grain size and width with process parameters have been well established in traditional fusion welding (Refs. 28, 29).

In FSW, Nelson et. al (Ref. 30) reported that peak temperatures in the HAZ and microhardness increased with increasing heat input in FSW HSLA 65. However, the extent to which the dependent variables influenced the microstructural evolution of FSW HSLA 65 weld is yet unknown. No correlation between dependent variables and microstructures has been established.

The objective of this study was to establish correlations between FSW process variables, both dependent and independent, and postweld microstructures in HSLA 65 steel.

Table 1 — Measured Chemical Composition of HSLA-65 Steel (Ref. 16)

Element	wt-%	Element	wt-%
C	0.081	Cr	0.15
Mn	1.43	Cu	0.26
Si	0.2	N	0.009
S	0.003	V	0.055
P	0.022	Ti	0.013
Ni	0.35	Nb	0.021
Mo	0.063	Al	0.018
Fe	Balance	Boron	<0.0005

Experiments

The chemical composition of the HSLA 65 (ASTM A945) used in this study is provided in Table 1. The base metal microstructure consists of refined upper bainite islands randomly embedded in the polygonal fine-grained ferrite matrix, with the average grain size about 8 μm as shown in Fig. 1.

Test plates were prepared from 9.5-mm-thick rolled plate with dimensions of 762 mm in length and 203.2 mm in width. The long axis of the test plate was parallel to the rolling direction. Each plate was lightly ground on both sides to remove oxide and surface scale prior to welding. Before welding, the plates were degreased with methanol. All welds were performed under a depth-controlled process. Partial penetration welds were made parallel to the plate rolling direction. Argon, at a flow rate of 1.1 m^3/h, was used as shielding gas to protect both the tool and the weld area from surface oxidation.

A convex-scrolled-shoulder-step-spiral (CS4) tool was used for all the welds. The shoulder and pin section of the tool are manufactured from solid PCBN (polycrystalline cubic boron nitride). The geometry of the CS4 tool is shown in Fig. 2. A 0.5-deg head tilt was applied during plunge and welding. All process parameters and torques were recorded during welding.

Trial experiments were conducted to determine the working range of rotation and welding speeds. Feasible limits of the parameters were chosen to ensure that the FSW joints were free from any defects. Design of experiments (DOE) techniques were used to form the design matrix. Nine experimental conditions are derived from full factorial experimental design matrix ($3^2 = 9$). The method of designing such a matrix is presented elsewhere (Refs. 38, 39). Table 2 shows the nine sets of FSW parameters used to form the design matrix. Fully consolidated welds were made at all parameters summarized in this table. The corresponding axial force and spindle torque are also shown in Table 2. The recorded spindle torque increases with increasing welding speed and decreasing rotation speed which is similar to that reported by Cui (Ref. 26).

Equations 1 and 2 were used to calculate the power and heat input, respectively.

$$P = \frac{(2\pi)\Omega T}{60} \quad (1)$$

$$HI = \frac{P}{v} \quad (2)$$

where P is power (kW); Ω is rotation speed (rev/min); T is recorded spindle torque by FSW machine (N.m); HI is heat

Table 2 — Average Heat Input Value for Each Process Parameter of HSLA-65 FSW (the bold parameters are selected to establish the correlations with post-weld microstructures)

Rotation Speed (rev/min)	Welding Speed (mm/min)	Axial-Force (kg)	Spindle Torque (N.m)	Power (kW)	Heat Input (kJ/mm)	Advance per Revolution (mm/rev)	Pseudo Heat Index (rev^2/mm)
300	**51**	**3410**	**90**	**2.8**	**3.33**	0.17	1772
300	127	4297	119	3.8	1.77	0.42	709
300	**203**	**4725**	**141**	**4.4**	**1.31**	0.68	443
450	51	3144	71	3.3	3.93	0.11	3986
450	127	3769	85	4.1	1.91	0.28	1594
450	203	3740	98	4.6	1.37	0.45	997
600	**51**	**3051**	**58**	**3.6**	**4.27**	0.08	7087
600	127	4970	76	4.8	2.25	0.21	2835
600	**203**	**3956**	**85**	**5.4**	**1.58**	0.34	1772

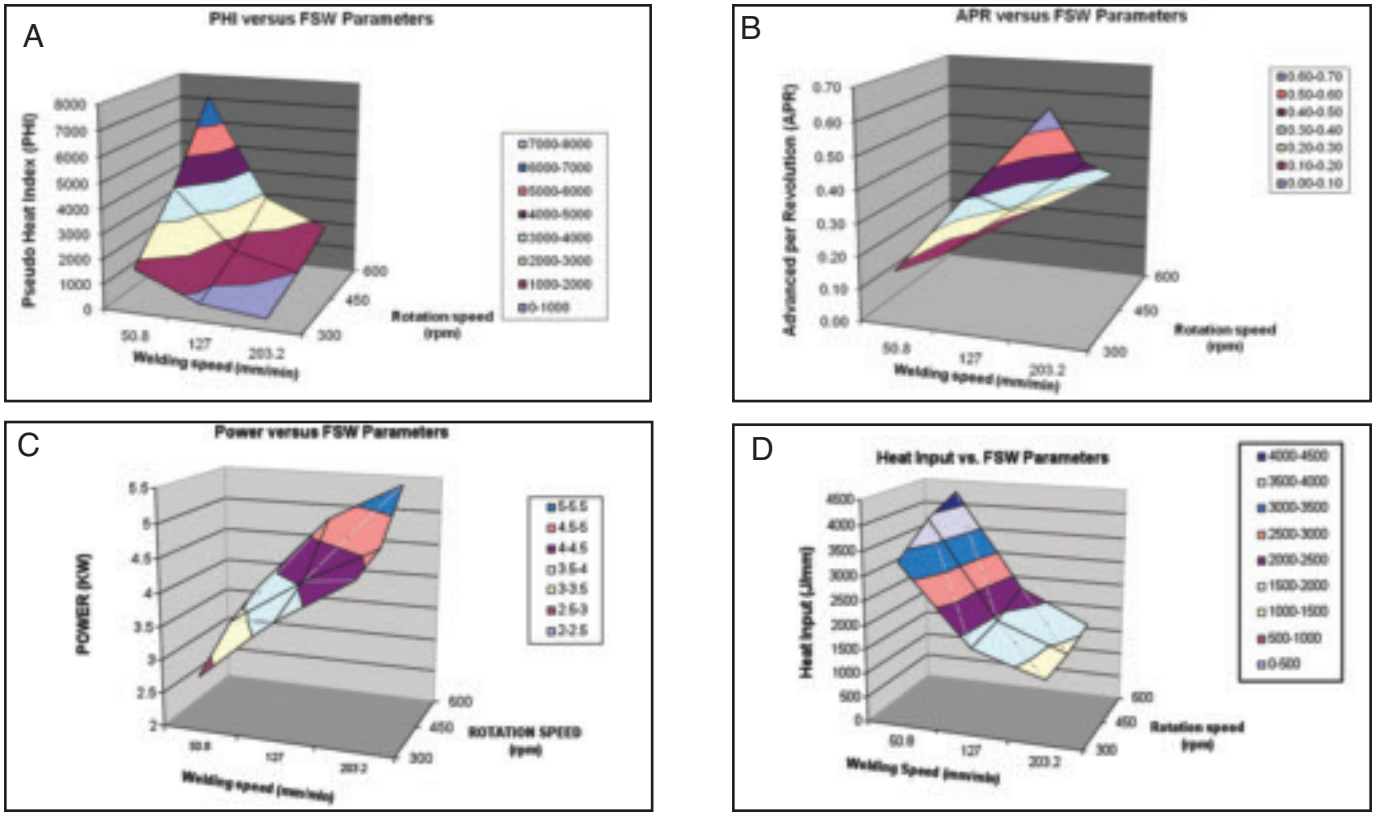

Fig. 3 — A— PHI; B — APR; C — power; D — heat input vs. FSW process parameters.

input (J/mm); and ν is welding speed (mm/min).

In order to establish correlations between postweld microstructures and FSW process variables, four different welding parameters (highlighted in bold text in Table 2) were chosen. The selected welding parameters covered the extreme and intermediate levels of power and heat input, based on the data in Table 2.

Transverse samples were removed from the welds for optical metallography analysis. Each sample was ground and polished successfully through 1-μm diamond paste. Samples were etched with 2% Nital and analyzed optically at magnifications up to 1000× using an Olympus GX51 microscope.

Results and Discussions

Relations between Independent and Dependent Variables in FSW

In order to correlate postweld microstructures with process variables, it is necessary to understand the relationship between FSW independent and dependent variables. In traditional arc welding, those relations have been well-established. Power and heat input are controlled directly by the independent variables, i.e., welding current, voltage, and travel speed (Ref. 28). Power and heat input have a linear relationship with these independent variables, e.g., increase with increasing welding voltage and current, and deceasing welding speed.

Friction stir welding is substantially different from arc welding. The independent variables in FSW include rotation speed, welding speed, axial force, tool geometry, and tool material. These variables can be directly controlled by the operator. Dependent process variables are heat input, power, and spindle torque. Unlike arc welding, power and heat input in FSW cannot be controlled directly by independent variables. Power is dependent on rotation speed and spindle torque. Spindle torque is not a controlled variable, but rather a response variable (Ref. 31). To complicate matters, spindle torque is a function of rotation speed, welding speed, tool geometry, tool material, and tool depth/axial force. Thus, it is difficult to develop simple relationships between independent and dependent variables in FSW.

Early FSW machines did not have the ability to monitor or record spindle torque. As a result, earlier researchers attempted to establish simple empirical relationships between input variables and machine outputs. Pseudo heat index (PHI) (Refs. 32–34) and advance per revolution (APR) (Ref. 31) were developed as parameter indexes to correlate with peak temperature and postmechanical properties. The PHI and APR are defined in Equations 3 and 4, respectively.

$$PHI = \frac{\Omega^2}{v} \quad (3)$$

$$APR = \frac{v}{\Omega} \quad (4)$$

Where Ω is rotation speed (rev/min), ν is welding speed (mm/min).

These indexes do not take into account the effect of spindle torque or capture the specific energy of the process. Given that postweld microstructures are strongly dependent on heat input in traditional arc welding (Refs. 28, 29), it would seem necessary to capture the effect of the specific energy in FSW. Therefore, it is likely that power and heat input will exhibit better correlation with postweld microstructures. The comparison of these parameter indexes in the following section provides additional evidence to identify the process index that correlates best with postweld microstructures.

Comparison of FSW Parameter Indexes

In order to illustrate the characteristics of PHI, APR, power, and HI (heat input), comparisons of these parameter indexes are discussed below. Using the data in Table 2, PHI, APR, power, and HI are plotted vs. FSW rotation speed and welding speed. These three-dimensional plots are shown in Fig. 3.

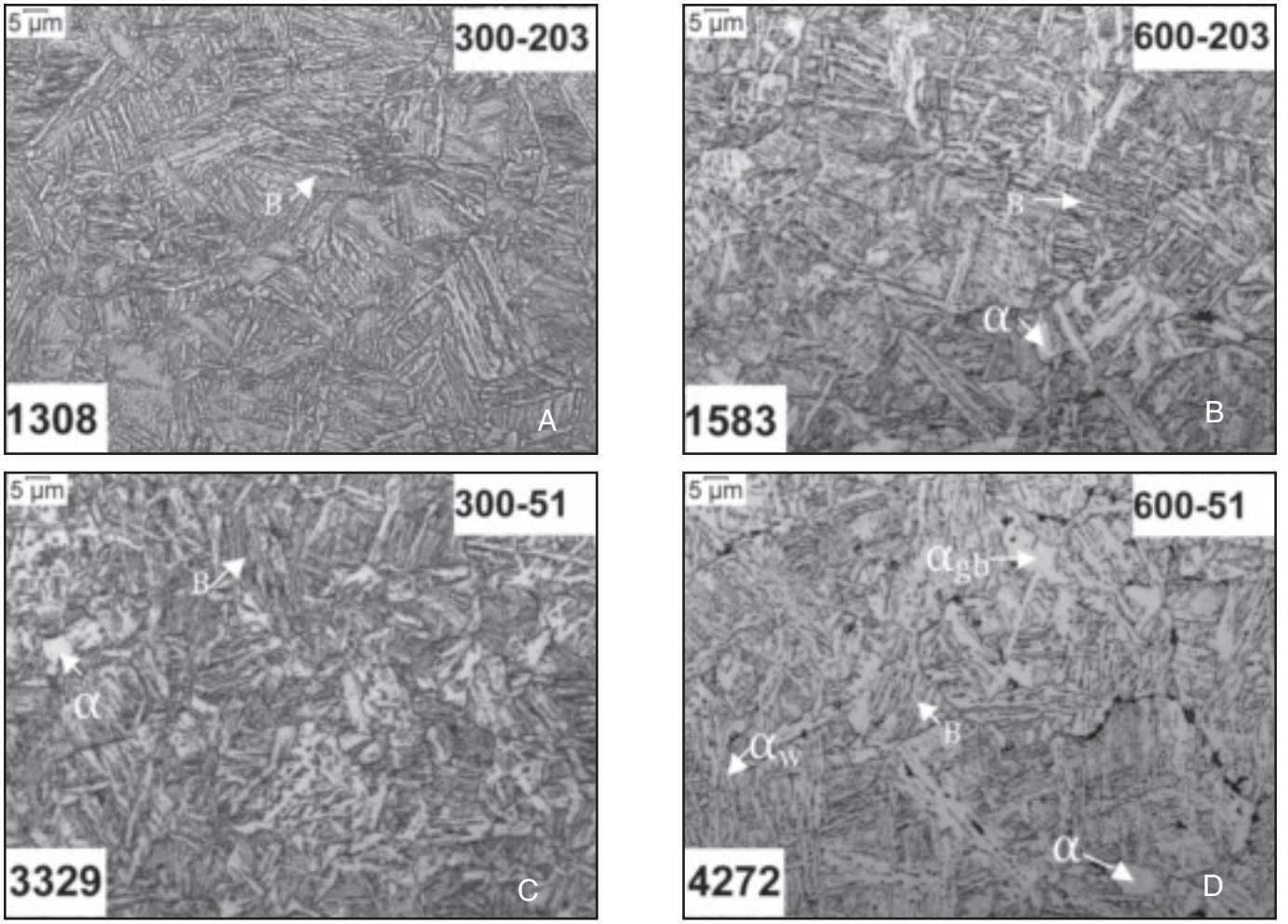

Fig. 4 — Microstructures of weld nugget center (NC) at various heat inputs (500×).

The PHI exhibits a second-order linear relationship with rotation speed and reciprocal relationship with welding speed as shown in Fig. 3A. The APR exhibits the linear relationship with welding speed and a reciprocal relationship with rotation speed as shown in Fig. 3B. These characteristics imply that APR is less complicated parameter index, since it has a lower order relationship than PHI.

Both PHI and APR are not unique in that multiple combinations of these indexes may have the same heat input. For example, in Fig. 3A, 600 rev/min-203 mm/min, and 300 rev/min-51 mm/min, have the same PHI values, but these two parameters have different power and heat inputs. The APR has similar redundancies. For example, 600 rev/min-203 mm/min has the same APR value as 300 rev/min-102 mm/min, but these have different heat inputs. Redundancies prevent accurate correlations between parameters and postweld microstructural features.

Power and heat input display nonlinear relationships with rotation speed and welding speed, as shown in Fig. 3C, D. This is similar to that reported by Pew (Ref. 35) in FSW Al Alloys 7075, 5083, and 2024. The nonlinear relationships exist because power and heat input are the function of spindle torque, and spindle torque, as discussed earlier, is a response variable.

The nonlinearity suggests that single or even two parameter investigations are inadequate to develop correlation between FSW process parameters and postweld microstructure and properties. In this study, four parameters were chosen to investigate correlations between postweld microstructural characteristics and process parameters in FSW HSLA-65. The parameters used for this aspect of the investigation are highlighted in bold in Table 2.

Effects of Process Variables on Microstructures in Nugget Center (NC)

Microstructures in NC

In this section, some consideration is given to postweld microstructural changes in the friction stir weld nugget at different heat inputs. The nugget center defined in this study is located at the vertical centerline of the stir zone, which has equal distances between the top surface and bottom of HAZ in the weld.

Figure 4 compares the microstructural features within the NC at various heat inputs. The tool rotation speed (rev/min) and welding speed (mm/min) are noted in the upper right-hand corner of each micrograph. Heat inputs are noted in the bottom left-hand corners. The symbols in these images represent different transformation products: α represents polygonal ferrite; α_{gb} represents grain boundary allotriomorphic ferrite; B represents bainite; and α_w represents Widmanstätten ferrite. From these optical images, several microstructural characteristics can be observed.

There is no evidence of base metal (BM) microstructures shown in Fig. 4. The equiaxed grains in BM have completely transformed to lath bainite with some polygonal/grain boundary ferrite. This indicates the weld nugget reached a peak temperature in excess of the A3, even at the lowest heat input 1.31 kJ/mm.

It is well known that microstructural changes in the weld are primarily affected by heating rate, peak temperature, and subsequent cooling (Ref. 36). Cooling rate is associated with heat input, i.e., lower heat input produces faster cooling rate (Ref. 36). At the lowest heat input in Fig.

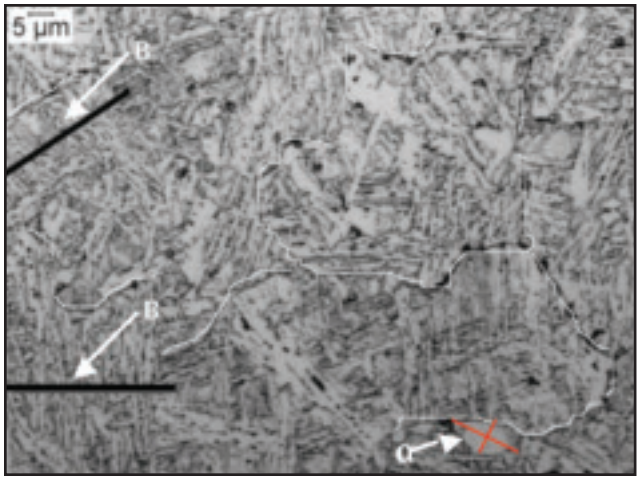

Fig. 5 — Schematic diagram shows how the ferrite grain and bainite lath measurements were made. B represents bainite, α represents polygonal ferrite. The red lines show the length of the short and long axes in polygonal ferrite grains; the ferrite grain size is obtained by averaging the length of the these two axes.

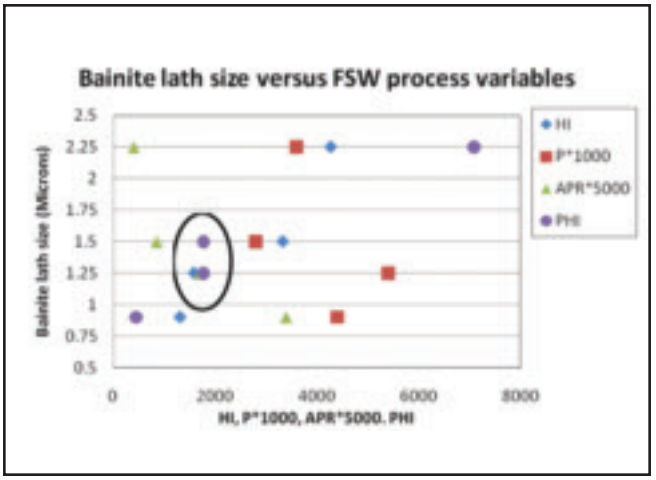

Fig. 6 — Bainite lath size vs. FSW process variables.

4A, the microstructure is mainly lath bainite. The lath boundaries are relatively straight and parallel.

With increasing heat input, two kinds of microstructures are formed (shown in Fig. 4B, C): polygonal ferrite and upper bainite. Higher heat input produces a slower cooling rate, and equiaxed polygonal ferrite starts to nucleate at the ferrite/austenite boundaries and extend into untransformed austenite grain interiors (Ref. 37).

In Fig. 4D, the highest heat input at 4.3 kJ/mm, the primary microstructures are lath bainite along with dispersed particles at prior austenite grain boundaries coexisting with some polygonal and allotriomorphic grain boundary ferrite. Allotriomorphic ferrite forms at a triple junction of prior austenite grain boundaries (Ref. 37). Long needle-shaped Widmanstätten ferrite is also observed in Fig. 4D. Pao (Ref. 20) has reported similar structures in the stir zone of FSW HSLA-65.

In summary, additional polygonal/allotriomorphic grain boundary ferrite forms with increasing heat input. Although higher-temperature transformation products (polygonal and allotriomorphic grain boundary ferrite) are formed at higher heat input, lath bainite is still the dominant microstructure in the FSW NC. This is due to the relatively fast cooling rate in FSW compared to arc welding. Faster cooling rates are the result of 1) lower heat input, and 2) the large heat sinking effect produced by the backing anvil.

Prior austenite grains (PAGs) are also visible in these figures. However, most of the PAG boundaries are discontinuous. The limited alloy addition in these type alloys result in limited segregation to the PAG boundaries. As a result, etchants are unable to attack the prior austenite grain boundaries (GBs) enough to produce sufficient contract to clearly identify them. Discontinuous PAG boundaries are highlighted by white curved lines in Fig. 5. Prior austenite grains are identified by the existing boundaries with some estimation.

In order to investigate correlations between microstructures in the NC and FSW process variables, quantitative grain/lath size measurements are needed. Since the prior austenite grain boundaries are absent for the most part, PAG measurements were not used in the present study for the correlations made. In addition, bainite lath size is difficult to quantify precisely by optical microscopy even at higher magnifications (up to 1000×) because some bainite lath structures are too fine to be distinguished under optical microscope. Therefore, grain/lath size in the FSW NC were measured as accurately as possible by optical microscopy. Bainite lath size was measured using the line intercept approach. The data presented represent an average of at least eight measurements from each weld section. Although bainite lath sizes may only be semiquantitative at best, they are repeatable and adequate for establishing the desired correlations.

Figure 5 illustrates how the ferrite grain and bainite lath measurements are made to acquire semiquantitative data. Bainite lath is measured by drawing a trace line (in black) of known length perpendicular to the lath boundaries, counting the numbers (N) of the lath intersections along this trace line, then dividing the line length by the number of intersections. Polygonal ferrite grains are easy to identify as shown in this figure. The measurements of ferrite grains were taken on every ferrite grain found in the optical images by averaging the length of the long and short axes as shown in Fig. 5.

The average grain/lath sizes are shown in Table 3. The ferrite grain size ranges from about 10 to 25 μm as heat input increases from 1.31 to 4.27 kJ/mm. Over this same range, bainite lath size increases from 0.9 to 2.25 μm. The authors believe the bainite laths observed in these images consist of several thinner laths that are difficult to distinguish by optical microscope. The lath sizes report may likely be larger than the actual value for reasons described previously.

Table 3 — Variation of Grain Size in the NC with Changing Power and Heat Input

Rotation Speed (rev/min)	Welding Speed (mm/min)	Power (kW)	Heat Input (kJ/mm)	Bainite Lath (μm)	Ferrite Grain Size (μm)	Width of HAZ (mm)
300	203.2	4.4	1.31	0.9	10	0.14
600	203.2	5.4	1.58	1.25	12.5	0.26
300	50.8	2.8	3.33	1.5	13	0.35
600	50.8	3.6	4.27	2.25	25	0.50

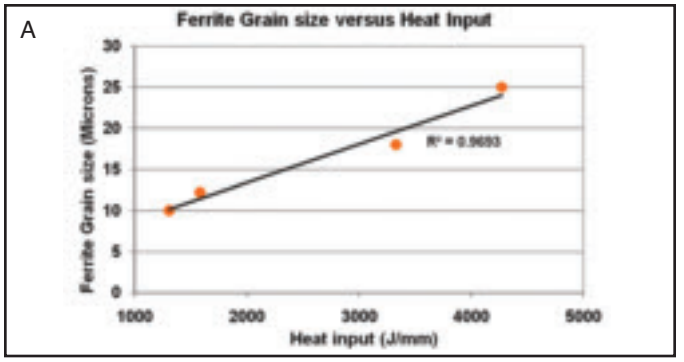

Fig. 7 — Variation of heat input vs. the following: A — Grain size; B — bainite lath size.

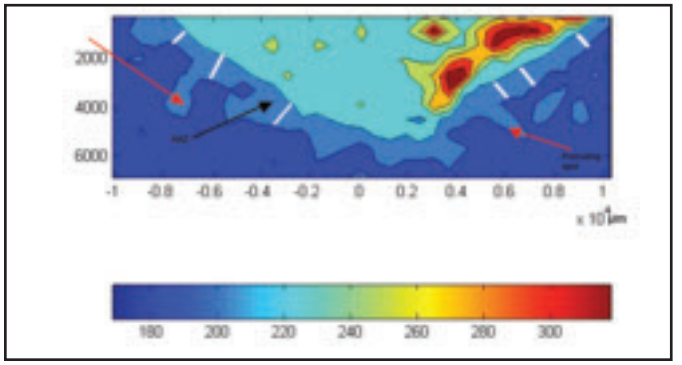

Fig. 8 — Weld hardness contour map at 600 rev/min-203 mm/min (1583 J/mm) shows the hardness distribution. The black arrow indicates the HAZ. The white lines indicate the measurement taken to obtain the average width of the HAZ. Red arrows indicate the protruding spots in the HAZ.

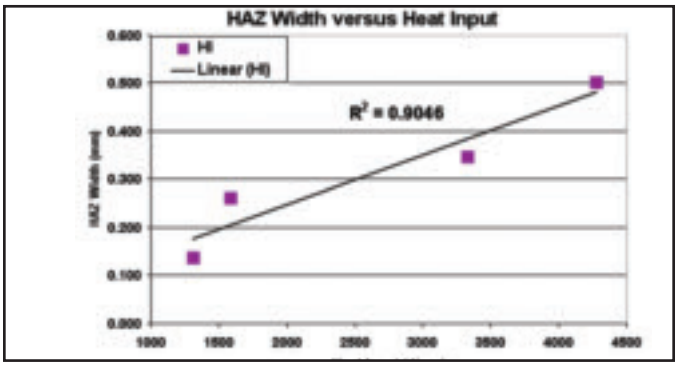

Fig. 9 — Width of HAZ vs. heat input

Correlate Postweld Microstructures with Process Variables

In this section, correlations between FSW process variables and postweld microstructures are investigated. Using the data in Table 3, the bainite lath size is plotted against PHI, APR, P, and HI to identify which FSW process index exhibits the best correlation with postweld microstructures. The weld indexes were scaled to fit on the same plot as shown in Fig. 6.

The PHI is not a unique FSW heat index. Both the 600 rev/min and 203 mm/min, and the 300 rev/min and 51 mm/min (circled in Fig. 6) have the same PHI but a 17% difference in bainite lath size. Contrary to most heat indexes, APR exhibits a nonlinear inverse relationship with bainite lath size, e.g., bainite lath size increases with decreasing APR. Additionally, power exhibits essentially no relationship with bainite lath size. Bainite lath size correlates best with HI, exhibiting a nearly linear increase with increasing HI. Additionally, HI is a unique heat index, capturing all elements of the process that contribute to the specific energy. The HI will be used as the FSW heat index through the remainder of this paper.

Using the data in Table 3, bainite lath and ferrite grain sizes were plotted against heat input — Fig. 7. Ferrite grain size (Fig. 7A) and bainite lath size (Fig. 7B) increase linearly with increasing heat input. With an increase in heat input of 2.27 kJ/mm, ferrite grain size and lath sizes increased 150% and 150%, respectively.

The width of the HAZ in a friction stir weld provides additional evidence of heat input dependence. The width measurement was obtained from a Vickers hardness map of the weld as shown in Fig. 8. The weld contour map clearly displays the HAZ as indicated by the black arrow in the map. The range of 200 to 205 Hv was selected as the value of hardness at which the HAZ width was measured. The region adjacent to the weld is the HAZ, which turns a light blue color in the hardness map. The HAZ width was measured at ten different locations as shown by the white lines drawn in Fig. 8 to obtain the average measurement. Some protruding spots (as indicated with red arrows in Fig. 8) in the HAZ do not represent the actual HAZ, which is HAZ with some softening spots in the base metal or bad hardness points. So measurements of the HAZ widths were not made at those protruding spots. In addition, the measurements were not taken at the bottom of the weld as the heat transfer was likely different at that location. The HAZ width as a function of HI is plotted and shown in Fig. 9. Similar to traditional arc welding (Refs. 28, 29), the width of the HAZ increases linearly with increasing heat input in FSW.

The linear relationship between bainite lath/ferrite grain sizes and heat input were established. Since the peak temperature and cooling rate are governed by the heat input in the FSW nugget center, higher heat input produces the following: 1) higher peak temperature above A_3 in the NC, and 2) slower cooling rate. Peak temperature strongly affects prior austenite grain size, i.e., higher peak temperature produces coarser austenite grains. This in turn would produce coarser microstructures at the same cooling rate since larger PAG size provides fewer nucleation sites (Ref. 39). This combined with slower cooling rate prompt the formation of larger grain/lath structures with increasing heat input.

In the present study, linear correlations between heat input and postweld microstructures in the FSW nugget center (NC) are established. Although the fit is good, the accuracy would likely improve if quantitative microstructural data were obtained. These efforts are currently under investigation.

Conclusions

The following conclusions can be made from this investigation:

1. Of the FSW process heat indexes investigated, heat input provided the best correlation with post-friction stir weld microstructures. Heat input exhibits a linear

relationship with ferrite grain size and bainite lath size.

2. Other process indexes (APR, PHI, and power) exhibit nonlinear relationships with postweld microstructures. The APR and PHI are not unique: e.g., different weld parameters can have the same index value.

3. Ferrite grain size and bainite lath size both increased 150% with an increase in heat input of 2.27 kJ/mm.

References

1. Dawes, C. J., and Thomas, W. M. 1995. *TWI Bull* 6: p. 138.

2. James, M., and Mahoney, M. 1999. *Proceedings of the First International Symposium on Friction Stir Welding*. Thousand Oaks, Calif., June 14–16.

3. Mohoney, M. V., Rhodes, C. G., Flintoff, J. G., Spurling, R. A., and Bingel, W. H. 1998. *Metall Mater Trans* 38: p. 703.

4. Rhodes, C. G., Mohoney, M. V., Bingel, W. H., Spurling, R. A., and Bampton, C. C. 1997. *Scripta Mater* 36: p. 69.

5. Jata, K. V., Sankaran, K. K., and Ruschau, J. J. 2000. *Metall Mater Trans* 31A: p. 2181.

6. Reynolds, A. P., Lockwood, W. D., and Seidel, T. U. 2000. *Mater. Sci. Forum* pp. 331–337, 1719–1724.

7. Thomas, W. M., et al. 1991. International Patent Application Number PCT/GB92/02203 and GB Application Number 9125978.8.

8. Juhas, M. C., Viswanathan, G. B., and Fraser, H. L. 2000. *Proceedings of the Second Symposium on Friction Stir Welding*, Gothenburg, Sweden, June.

9. Park, H. S., Kimura, T. K., Murakami, T., Nagano, Y., Nakata, K., and Ushio, M. 2004. Microstructure and mechanical properties of friction stir welds of 60%Cu-40%Zn copper alloy. *Mater, Sci. Eng. A* 371: 160–169.

10. Lee, W. B., and Jung, S. B. 2004. The joint properties of copper by friction stir welding. *Mater. Lett.* 58: 1041–1046.

11. Cui, L., Fujii, H., Tsuji, N., Nakata, K., Nogi, K., Ikeda, R., and Matsushita, M. 2007. Transformation in stir zone of friction stir welded carbon steels with different carbon contents. *ISIJ International* Vol. 47, No. 2, pp. 299–306.

12. Ueji, R., Fujii, H., Cui, L., Nishioka, A., Kunishige, K., and Nogi, K. 2006. Friction stir welding of ultrafine plain low-carbon steel formed by the martensite process. *Materials Science & Engineering A* 423: 324–330 4 6.

13. Fujii, H., Cui, L., Tsuji, N., Maeda, M., Nakata, K., and Nogi, K. 2006. Friction stir welding of carbon steels. *Materials Science and Engineering A* 429: pp. 50–57.

14. Posada, M., Deloach, J., Reynolds, A. P., Skinner, M., and Halpin, J. P. 2001. Friction stir weld evaluation of HH-36 and stainless steel weldment. *Friction Stir Welding and Processing*, Indianapolis, Ind., Nov. 4–8. pp. 159–171.

15. Sato, Y. S., Nelson, T. W., Sterling, C. J., Steel, R. J., and Pettersson, C. O. 2005. Microstructure and mechanical properties of friction stir welded SAF 2507 superduplex stainless steel. *Materials Science & Engineering A* 397: pp. 376–384.

16. Sampath, K. 2006. An understanding of HSLA-65 plate steels. *Journal of Materials Engineering and Performance*, Volume 15(1) February: 32–40.

17. Konkol, P. J., Mathers, J. A., Johnson, R., and Pickerns, J. R. 2003. Friction stir welding of HSLA-65 steel for shipbuilding. *Journal of Ship Production*, Vol. 19, No. 3, August: 159–164.

18. Ozekcin, A., Jin, H. W., Koo, J. Y., Bangaru, N. V., and Ayer, R. 2004. A microstructural study of friction stir welded joints of carbon steels. *International Journal of Offshore and Polar Engineering*, Vol. 14, No. 4, December.

19. Nelson, T. W., Su, J. Q., and Steel, R. J. 2004. Friction stir welding of ferritic steels. *Proceedings of ISOPE-2004: Fourteenth International Offshore and Polar Engineering Conference.*

20. Pao, P. S., Fonda, R. W., Jones, H. N., Feng, C. R., and Moon, D. W. 2007. Friction stir welding of HSLA-65 steel. TMS Annual Meeting & Exhibition, Orlando, Fla. *Friction Stir Welding and Processing IV*, pp. 243–251.

21. Posada, M., DeLoach, J., Reynolds, A. P., Fonda, R., and Halpin, J. 2003. Evaluation of friction stir welded HSLA-65. *4th International Friction Stir Welding Symposium*, Park City, Utah.

22. Querin, J. A., Davis, A. M., and Schneider, J. A. 2007. Effect of processing parameters on microstructure of the FSW nugget. TMS Annual Meeting & Exhibition, Orlando, Fla. *Friction Stir Welding and Processing IV*, pp. 185–192.

23. Rodrigues, D. M., Loureiro, A., Leitao, C., Leal, R. M., Chaparro, B. M., and Vilaca, P. 2009. Influence of friction stir welding parameters on the microstructural and mechanical properties of AA 6016-T4 thin welds. *Materials and Design* 30: pp. 1913–1921.

24. Afrin, N., Chen, D. L., Cao, X., and Jahazi, M. 2008. Microstructure and tensile properties of friction stir welded AZ31B magnesium alloy. *Materials Science and Engineering A* 472: pp. 179–186.

25. Cao, X., and Jahazi, M. 2009. Effect of welding speed on the quality of friction stir welded butt joints of a magnesium alloy. *Material and Design* 30: 2033–2042 4 7.

26. Cui, S., and Chen, Z. W. 2009. Effects of rotation speed and welding speed on material flow and stir zone formation during FSW/P. *Friction Stir Welding and Processing V*, TMS Annual Conference, pp. 125–133.

27. Adam, L., Pilchak, Z., Li, T., Fisher, J. J., Reynolds, A. P., Juhas, M. C., and Williams, J. C. 2007. The relationship between friction stir process (FSP) parameters and microstructure in investment cast Ti-6Al-4V. *Friction Stir Welding and Processing IV*, pp. 419–428.

28. Gunaraj, V., and Murugan, N. 1999. Prediction and comparison of the area of the heat-affected zone for the bead-on-plate and bead-on-joint in submerged arc welding of pipes. *Journal of Materials Processing Technology* 95: pp. 246–261.

29. Quan, Y. J., Chen, Z. H., Gong, X. S., and Yu, Z. H. 2008. Effects of heat input on microstructure and tensile properties of laser welded magnesium alloy AZ31. *Materials Characterization* 59: pp. 1491–1497.

30. Nelson, T. W., Anderson, S. J., and Segrera, D. J. 2007. Friction stir welding of X-65 steel. TMS Annual Meeting & Exhibition, Orlando, Fla. *Friction Stir Welding and Processing IV*, pp. 269–277.

31. Reynolds, A. P. *Microstructure Development in Aluminum Alloy Friction Stir Welds*. *Friction Stir Welding Processing*, Chapter 4, pp. 51–70.

32. Arbegast, W. 2003. *Hot Deformation of Aluminum Alloys III*. TMS, Warrendale, Pa., pp. 313–327.

33. Sanders, D., Edwards, P., Grant, G., Ramulu, M., and Reynolds, A. 2008. Superplastically formed friction stir welded tailored aluminum and titanium blanks for aerospace applications. *6th EuroSPF Conference*, Carcassonne, France.

34. Balasubramanian, N., Gattu, B., and Mishra, R. S. 2009. *Science and Technology of Welding and Joining*, Vol. 14, No. 2, pp. 141–145.

35. Pew, J. W., Nelson, T. W., and Sorensen, C. D. 2007. *Development of a Torque-based Weld Power Model for Friction Stir Welding. Friction Stir Welding and Processing IV*, pp. 73–82.

36. Patchett, B. M., Bringas, J. E., and Thomas, R. D. *The Metals Blue Book*, pp. 18, 19.

37. Grong, Ø. *Metallurgical Modeling of Welding*, 406-45038. L.Y. Wei and T. W. Nelson. Influence of heat input on microstructural and mechanical properties of friction stir welded HSLA-65 steel.

38. Box, G. E. P., Hunter, W. H., and Hunter, J. S. 1978. *Statistics for Experiment.* New York, N.Y.: John Wiley Publications.

39. Elangovan, K., Balasubramanian, V., and Babu, S. 2009. Predicting tensile strength of friction stir welded AA 6061 aluminum alloy joints by a mathematical model. *Materials and Design* (30): pp. 188–193.